Chapter 5

RESULTS & DISCUSSION

5.1 CONCENTRATION PROFILES

Concentration profiles in a battery system are very important in order to measure the performance of the battery system. To obtain concentration profiles, there are several aspects that need to be considered such as governing equations (chapter 3), method of solution (chapter 4) and suitable value of parameters. In this study, Theta formulation under the FDM has been used for all three schemes, that is explicit $(\alpha = 0)$, implicit $(\alpha = 1)$ and Crank Nicolson $(\alpha = 0.5)$. In order to make comparison, the values of parameters used in this work are taken to be similar with those used by Doyle and Newman (1997) as listed in table 5.1.

Table 5.1: Parameters and values used by Doyle and Newman (1997).

Parameter (Unit)	Value
Porosity of electrode, ε	0.5
Diffusion of coefficient, D (cm^2/s)	7.5×10^{-8}
Faraday's constant, F (C/mol)	96487 (standard)
Initial concentration, c_o (mol/cm^3)	2×10^{-3}
Transference number, t_+^0	0.2
Thickness of separator, δ_s (cm)	50×10^{-4}
Thickness of cathode, δ_c (cm)	200×10^{-4}

Figure 5.1 gives the concentration profiles for the three schemes under different discharge current density of I = 0.5, 1.0 and 1.39 mA/cm^2. The profile from Doyle and Newman (1997) was plotted together for comparison as follows

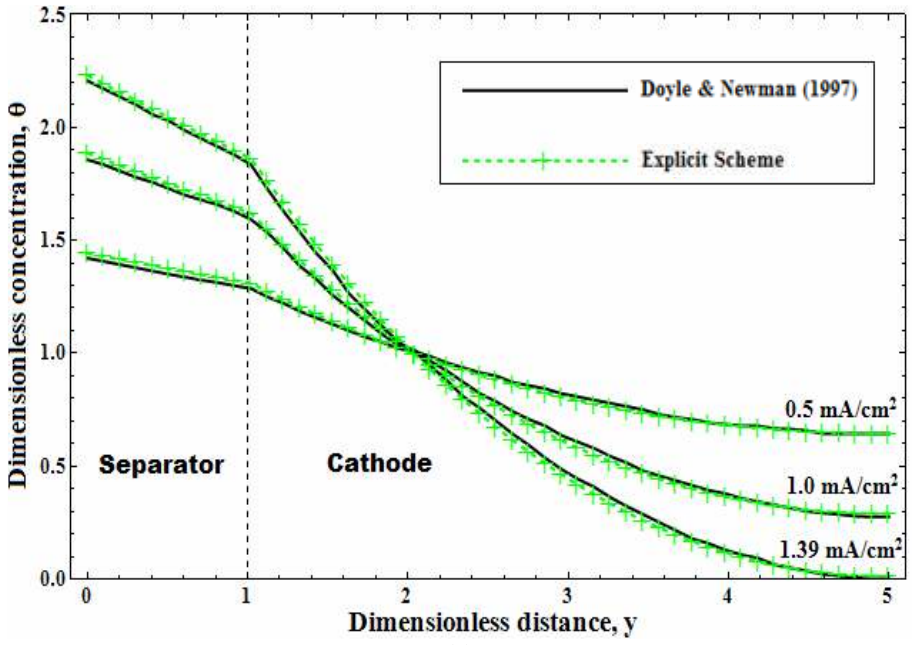

(a)

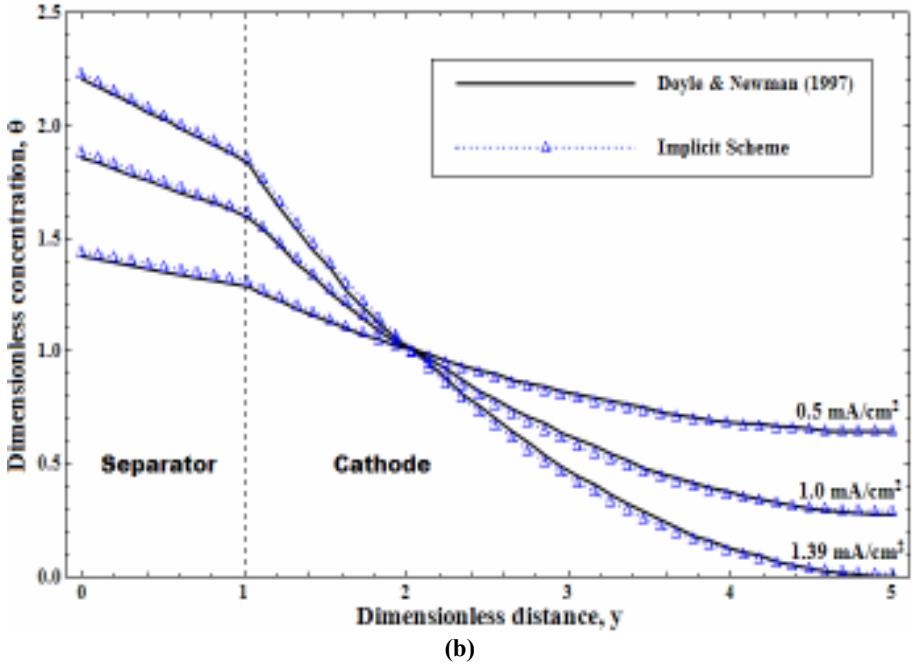

(b)

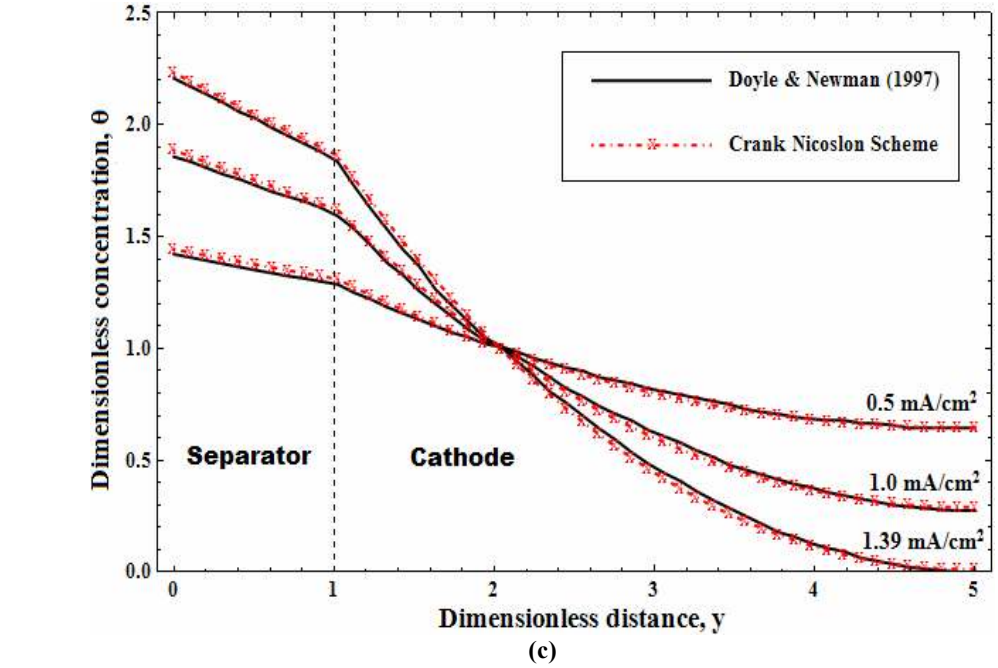

(c)

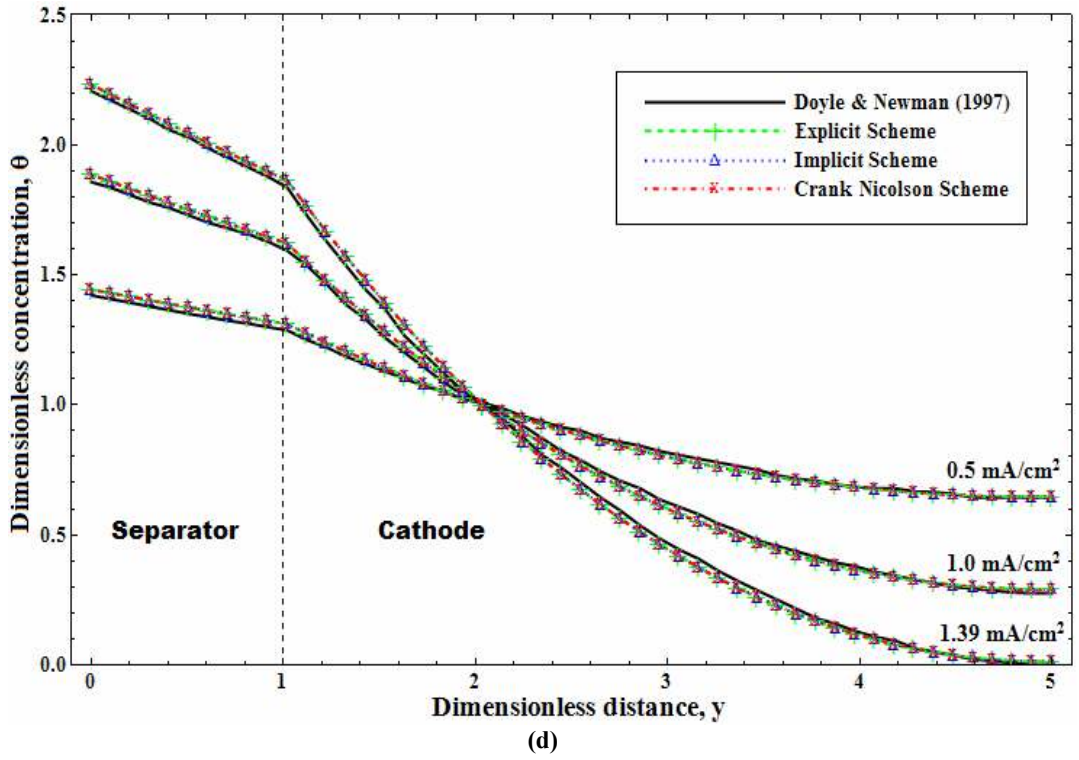

(d)

Figure 5.1: Concentration profile using three schemes of Theta Formulation under FDM compared with Doyle and Newman (1997) at different discharge currents. (a) explicit scheme, (b) implicit scheme, (c) Crank Nicolson scheme and (d) Doyle and Newman (1997) with three schemes together.

Figure 5.1(a) shows the concentration profiles for the explicit scheme under different discharge currents of I = 0.5, 1.0 and 1.39 mA/cm^2 compared to the profile obtained from Doyle and Newman (1997). For explicit scheme, figure 5.1(a) shows the initial dimensionless concentration during low discharge current (0.5 mA/cm^2) is 1.44312, intermediate discharge current (1.0 mA/cm^2) is 1.88630 and high discharge current (1.39 mA/cm^2) is 2.23196. At y = 5, the final dimensionless concentration during low discharge current is 0.64494, intermediate discharge current is 0.29001 and high discharge current is 0.01312.

Figure 5.1(b) shows the concentration profiles for the implicit scheme under different discharge current of I = 0.5, 1.0 and 1.39 mA/cm^2 compared to those reported by Doyle and Newman (1997) work. In this figure, implicit scheme gives the initial dimensionless concentration during low discharge current (0.5 mA/cm^2) equals to 1.44315, whereas the intermediate discharge current (1.0 mA/cm^2) equals to 1.88624 and high discharge current (1.39 mA/cm^2) equals to 2.23187. The final dimensionless concentration at y = 5 during low discharge current is 0.64501 while 0.28987 during intermediate discharge current and 0.01292 during high discharge current.

Figure 5.1(c) shows the concentration profiles for the Crank Nicolson scheme under different discharge currents of I = 0.5, 1.0 and 1.39 mA/cm^2 compared to those from Doyle and Newman (1997) studies. For figure 5.1(c), the initial concentration at y = 1 during low discharge current (0.5 mA/cm^2) is equal to 1.44314 while 1.88627 during intermediate discharge current (1.0 mA/cm^2) and 2.23192 during high discharge current (1.39 mA/cm^2). For final dimensionless concentration at y = 5 during low

discharge current is 0.64497, intermediate discharge current is 0.28994 and high discharge current is 0.01302.

From these three figures; figure 5.1(a), figure 5.1(b) and figure 5.1(c), all concentration profiles were plotted in one figure as shown in figure 5.1(d). Hence, figure 5.1(d) shows the concentration profile for the three schemes under different discharge currents of I = 0.5, 1.0 and 1.39 mA/cm^2 together with the results obtained by Doyle and Newman (1997). In figure 5.1(d), all the concentration profiles show linear slope decreased until they reached the dashed line at y = 1, which is the separator/cathode interface. Then, these concentration profiles continue to decrease after y = 1 until y = 5 but now have a quadratic shape slope. These concentration profiles and Doyle and Newman's profiles intersect at y = 2.

These decreasing shapes are reasonable because during full charge, lithium-ions must fulfill the front of the separator (anode was assumed as lithium foil), while the lithium-ion concentration which is higher at the front of separator. During discharge process, lithium-ions deplete across the battery, which resulted the lithium-ion concentration becoming lower at the back of the cathode because the lithium-ions have dissolved through chemical reaction in cathode. In addition, the difference between initial and final concentration defines the concentration depletion rate. Hence, from figure 5.1(d), the depletion rate is higher when the discharge current increases. This can be seen during high discharge current (1.39 mA/cm^2), that the decreasing slope is steeper (the difference between initial and final concentration is higher) than low discharge current (0.5 mA/cm^2). The important observation from figure 5.1 is that the concentration profiles solved by all of these three schemes for three different discharge currents are similar to the Doyle and Newman (1997) work.

Figure 5.2 gives the concentration profile for the three schemes together with the result obtained by Subramanian and White (2001) work. For comparison, we have taken the dimensionless time as $\tau = 1$, similar to Subramanian and White (2001). The value for applied current, J is assumed as -1 and the value for porosity of electrode, ε is assumed equal to 0.35.

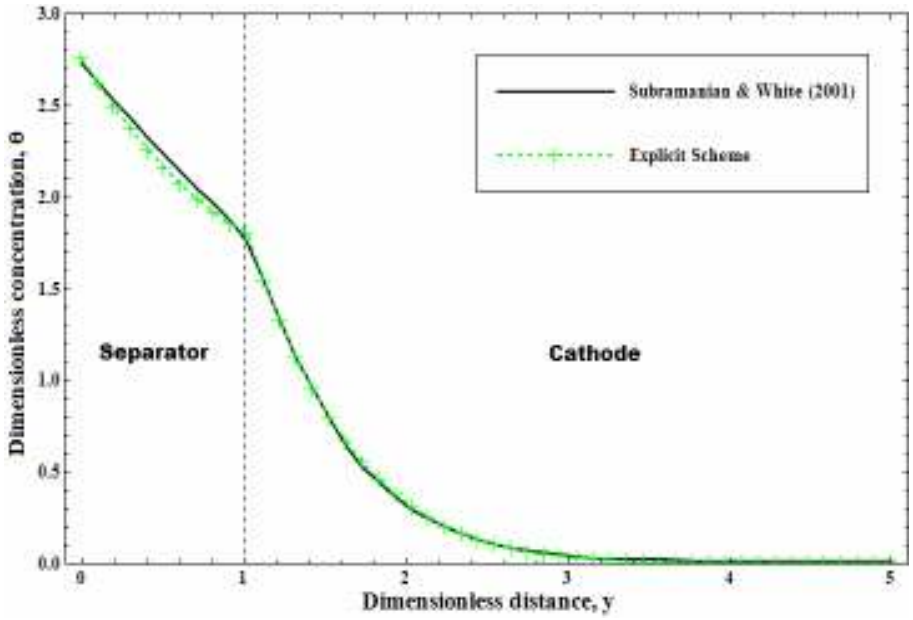

(a)

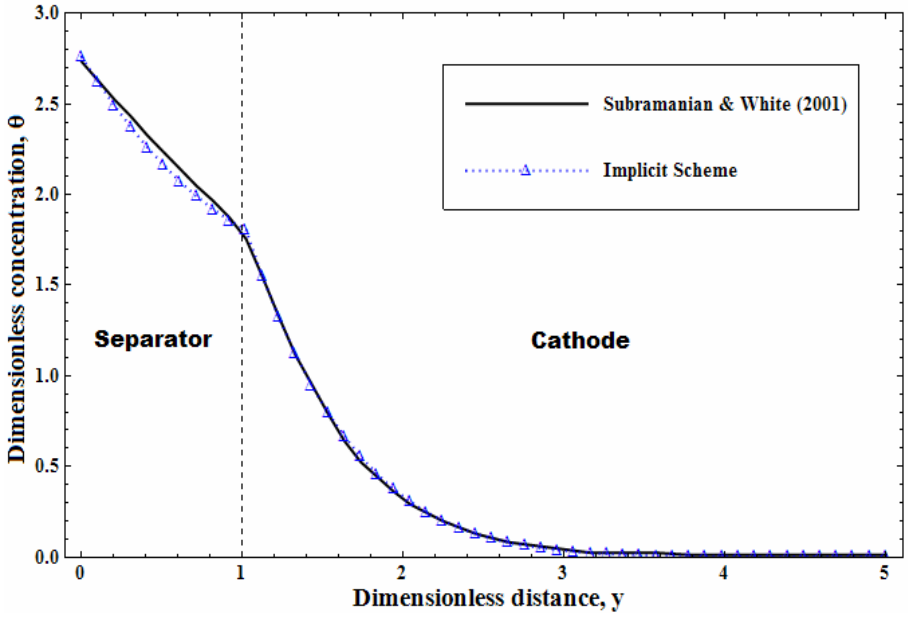

(b)

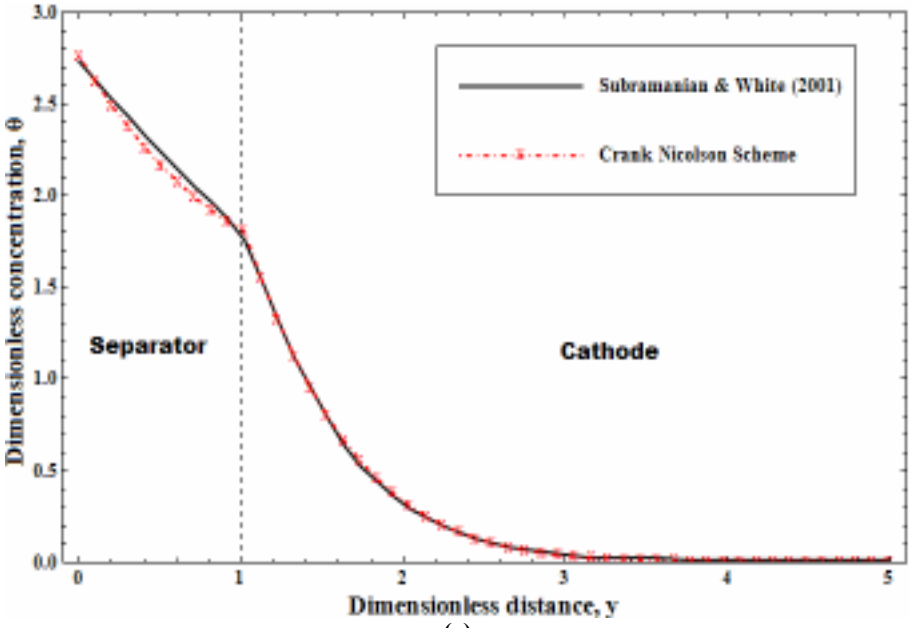

(c)

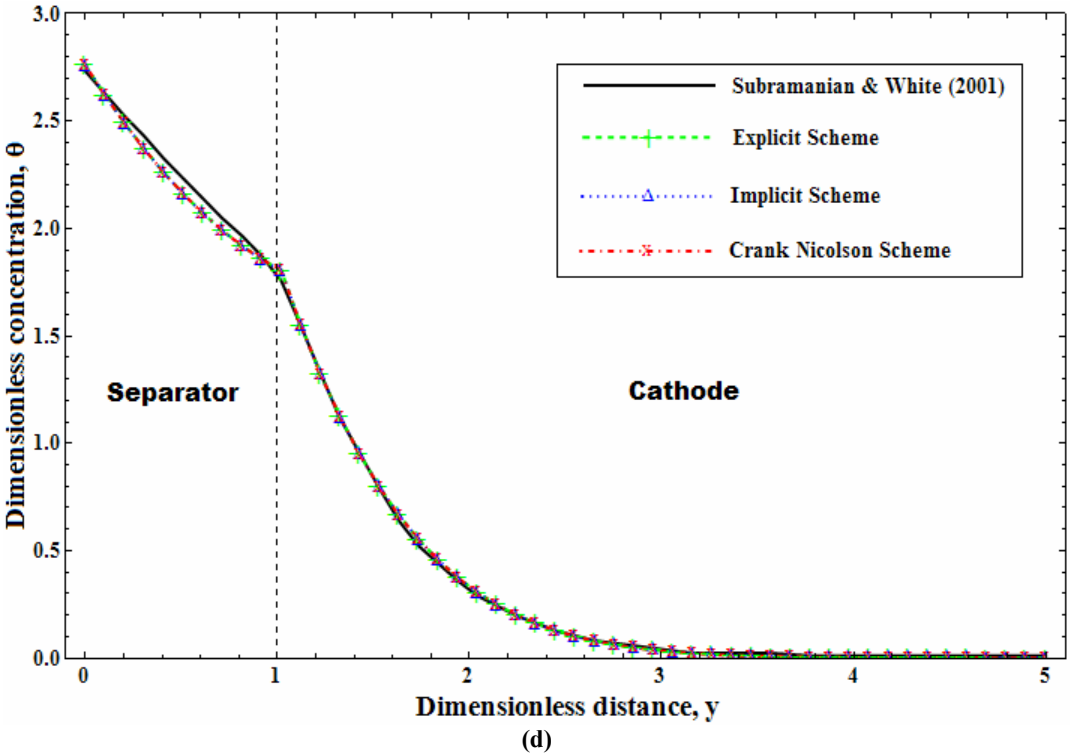

(d)

Figure 5.2: Concentration profile using three schemes of Theta Formulation under FDM compared with Subramanian and White (2001) at applied current, $J = -1$. (a) explicit scheme, (b) implicit scheme, (c) Crank Nicolson scheme and (d) Subramanian and White (2001) with three schemes together.

Figure 5.2(a) shows the concentration profile for the explicit scheme while figure 5.2(b) for the implicit scheme and figure 5.2(c) for Crank Nicolson scheme. These three concentration profiles for three difference schemes in figure 5.2(a), figure 5.2(b) and figure 5.2(c) are plotted together with concentration profile from Subramanian and White (2001) study in figure 5.2(d). From figure 5.2(a), the explicit scheme gives the initial dimensionless concentration of 2.76055 and its final dimensionless concentration is equal to 0.00113. Meanwhile, figure 5.2(b) shows that the initial dimensionless concentration using implicit scheme is 2.75966 while the final dimensionless concentration is 0.00112. Otherwise, figure 5.2(c) gives the initial dimensionless concentration using Crank Nicolson scheme equal to 2.76011 and final dimensionless concentration equal to 0.00113. Then, figure 5.2(d) shows the summarization concentration profile using three schemes together with concentration profile from Subramanian and White (2001). The shape of the graphs from the three schemes compared to the shape of the graph form Subramanian and White (2001) study are in agreement, which is linear decreasing slope from $y = 0$ to $y = 1$ and quadratic decreasing slope from $y = 1$ to $y = 5$.

Figure 5.1 and figure 5.2 shows the concentration profiles from the three schemes of FDM are comply with concentration profile of Doyle and Newman (1997) and Subramanian and White (2001) works, respectively. In order to find the best scheme among these three schemes; explicit scheme, implicit scheme and Crank Nicolson scheme, we will use the result from Doyle and Newman's (1997) work. This is because the value of parameters used in Doyle and Newman (1997) work was given with more detail compared to Subramanian and White (2001) study.

5.2 EFFECTIVENESS AND ACCURACY

Before we can find the best scheme using several statistical tests, we must check the validity of our results. This is done by checking whether the result from these three schemes show significant difference with Doyle and Newman (1997) work or not. In order to check this significant difference, the significant test or known as *t*-test has been used. From chapter 4 we know that for $\frac{1}{2} \le \alpha \le 1$, Theta formulation is unconditionally stable, means that there is no condition to choose the value of *h* or *k*. Beside that, for $0 \le \alpha < \frac{1}{2}$ Theta formulation is conditionally stable. The condition that needs to be fulfilled is $(1-\alpha)\frac{\varepsilon^{\frac{1}{2}}k}{h^2} < 0.5$. Hence, from this condition, for this significant difference test the value of *h* is fixed and several values of *k* were used within a fixed interval $0.0005 \le k \le 0.1$. The result of the *p* value from this significant test is shown in table 5.2.

Table 5.2 shows the result of the *p* value from the *t*-test using three schemes for different discharge currents compared to Doyle and Newman (1997) at 5 minutes of discharge time. Statistically, the *p* value must not be below 0.05 in order to show that there is no significant difference between the two comparison data within 95% confidence interval. In this work this comparison data is referred to comparison between two concentration profiles. Hence, from table 5.2, all *p* values for implicit scheme and Crank Nicolson scheme during different discharge currents of I = 0.5, 1.0 and 1.39 mA/cm^2 are greater than 0.05. This means the concentration profile from this work using implicit scheme and Crank Nicolson scheme have no significant difference compared to (Doyle and Newman 1997) work within the 95% confidence interval. However, for explicit scheme ($\alpha = 0$) during discharge current of I = 0.5, 1.0 and 1.39 mA/cm^2, the *p* value is greater than 0.05 at *k* equal to 0.0005, 0.001 and 0.005 because at *k* equal to 0.01, 0.05 and 0.1 the Theta formulation is unstable according to condition $(1-\alpha)\frac{\varepsilon^{\frac{1}{2}}k}{h^2} < 0.5$. So for explicit scheme, the comparison of the concentration profile for significant difference with Doyle and Newman (1997) work is done only at *k* equal to 0.0005, 0.001 and 0.005. Hence, there is no significant difference between concentration profile using explicit scheme compare to concentration profile from Doyle and Newman (1997) work.

From table 5.2, it is seen that there is no significant difference between concentration profiles from Theta formulation (explicit scheme, implicit scheme and Crank Nicolson scheme) with concentration profile obtained from Doyle and Newman (1997). Hence, there must be one scheme that is more effective and accurate. In this study, the Root Mean Square Error (RMSE) will be used to evaluate the effectiveness

and accuracy of the solution using the three schemes in Theta formulation of FDM from Doyle and Newman (1997) study. RMSE according to Committee (1998) is defined as the square root of the average of the set of squared differences between dataset coordinate values and coordinate values from an independent source of higher accuracy for identical points. Most of the articles and books (Son 2008; Du et al. 2010; Irimia et al. 2010; Sethi et al. 2010) stated that RMSE as follows

$$\text{RMSE} = \sqrt{\frac{1}{n}\sum_{i=1}^{n}\left(y_i - x_i\right)^2} \qquad \text{----------(5.1)}$$

In this study, y_i is the Doyle and Newman (1997) data, x_i are the data from FDM scheme and n is the number of data. Table 5.3 shows the result for RMSE compared to Doyle and Newman (1997).

Table 5.3 shows the RMSE results comparison amongst the concentration profiles using three schemes under Theta formulation with concentration profile from Doyle and Newman (1997). This comparison was done during 5 minutes of discharge for different discharge currents I = 0.5, 1.0 and 1.39 mA/cm^2 at several value of *k* (this comparison work considered fixed value of *h*). The explicit scheme (α = 0), must be fulfill the condition that $(1-\alpha)\frac{\varepsilon^{\frac{1}{2}}k}{h^2} < 0.5$. Thus, for the fixed value of *h*, the explicit scheme shows the unstable result when *k* is equal to 0.01, 0,05 and 0.1. Hence for explicit scheme, the concentration profile result at *k* equal to 0.0005, 0.001 and 0.005 are taken to compare with concentration profile from Doyle and Newman (1997).

From table 5.3, we can see that for each discharge current (I = 0.5, 1.0 and 1.39 mA/cm^2) using implicit scheme, the RMSE is smaller when bigger values of *k* are used. For example, RMSE using implicit scheme during I = 0.5, 1.0 and 1.39 mA/cm^2 at *k* = 0.0005 are equal to 0.0153175, 0.0189742 and 0.0227318, respectively. However RMSE using implicit scheme during I = 0.5, 1.0 and 1.39 mA/cm^2 at *k* = 0.1 is equal to 0.0141028, 0.0172434 and 0.0200874, respectively. These trends are also similar for Crank Nicolson scheme, where RMSE is smaller when bigger values of *k* are used. For example, RMSE using Crank Nicolson scheme during I = 0.5, 1.0 and 1.39 mA/cm^2 at *k* = 0.0005 are equal to 0.0153177, 0.0189757 and 0.0227347, respectively. Then, RMSE using Crank Nicolson scheme during I = 0.5, 1.0 and 1.39 mA/cm^2 at *k* = 0.1 is equal to 0.0143112, 0.0180712 and 0.0215345, respectively. Meanwhile, for explicit scheme, we can see the different trend compared to implicit scheme and Crank Nicolson scheme trend. For explicit scheme, the trend shows that RMSE is smaller when we use the smaller value of *k*. For example, RMSE using explicit scheme during I = 0.5, 1.0 and

1.39 mA/cm^2 at k = 0.0005 are equal to 0.0153180, 0.0189773 and 0.0227376, respectively. Then, RMSE using explicit scheme during I = 0.5, 1.0 and 1.39 mA/cm^2 at k = 0.005 is equal to 0.0152676, 0.0189227 and 0.0226649, respectively.

In RMSE statistical test, the smallest value of RMSE indicates the best scheme. Hence, from table 5.3, implicit scheme gives the smallest RMSE compare to the two other schemes. This smallest error is at k = 0.1. Hence, we can conclude that by using RMSE, the most effective and accurate scheme is implicit scheme.

Furthermore, in order to evaluate the effectiveness and accuracy of the three schemes, the Mean Absolute Error (MAE) was also used. According to Willmott and Matsuura (2005) MAE is better than RMSE. MAE is define as follows

$$\text{MAE} = \frac{1}{n}\sum_{i=1}^{n}|y_i - x_i| \qquad \text{----------(5.2)}$$

where y_i is the Doyle and Newman (1997) data, x_i is the data from FDM scheme and n is the number of data. Table 5.4 shows the result for MAE compared to Doyle and Newman (1997).

Table 5.4 shows the MAE results comparison amongst concentration profile using three schemes under Theta formulation with concentration profile from Doyle and Newman (1997). This comparison was done during 5 minutes of discharge for different discharge current I = 0.5, 1.0 and 1.39 mA/cm^2 at several value of k (this comparison work considered fixed value of h). Similarly, for explicit scheme, concentration profile result at k equal to 0.0005, 0.001 and 0.005 is taken to compare with concentration profile from Doyle and Newman (1997) because at k equal to 0.01, 0.05 and 0.1 the concentration profile result are unstable.

From table 5.4, it can be seen that for each discharge current (I = 0.5, 1.0 and 1.39 mA/cm^2) using implicit scheme the MAE is smaller when the bigger value of k used. For example, MAE using implicit scheme during I = 0.5, 1.0 and 1.39 mA/cm^2 at k = 0.0005 are equal to 0.0130571, 0.0176816 and 0.0206717, respectively. However MAE using implicit scheme during I = 0.5, 1.0 and 1.39 mA/cm^2 at k = 0.1 is equal to 0.0120150, 0.0160033 and 0.0183432, respectively. These trends are also similar for Crank Nicolson scheme, where MAE is smaller when bigger value of k is used. For example, MAE using Crank Nicolson scheme during I = 0.5, 1.0 and 1.39 mA/cm^2 at k = 0.0005 are equal 0.0130590, 0.0176827 and 0.0206751, respectively. Then, MAE using Crank Nicolson scheme during I = 0.5, 1.0 and 1.39 mA/cm^2 at k = 0.1 is equal to 0.0124418, 0.0162328 and 0.0187978, respectively. Meanwhile, for explicit scheme, the trend shows that MAE is smaller when we use the smaller value of k. For example, MAE using explicit scheme during I = 0.5, 1.0 and 1.39 mA/cm^2 at k = 0.0005 are equal to 0.0130609, 0.0176838 and 0.0206785, respectively. Then, MAE using explicit scheme during I = 0.5, 1.0 and 1.39 mA/cm^2 at k = 0.005 is equal to 0.0130483, 0.017626 and 0.0206265, respectively.

Similar to the RMSE, the smaller the value of MAE indicates the best scheme. Hence, from table 5.4, implicit scheme gives the smallest MAE compared to two other schemes. This smallest error is at $k = 0.1$. Hence, we can conclude that MAE shows that the implicit scheme is the most effective and accurate scheme compare to explicit scheme and Crank Nicolson scheme.

Generally, the explicit scheme offers the easiest way to implement computer coding and give the fastest computational time to solve the several systems of equation compared to implicit scheme and Crank Nicolson scheme. According to Recktenwald (2011), the problem in one space dimension like in this study, the difference in computational time is not too important. Despite the fact that computational time using implicit scheme are much greater than explicit scheme but the superior stability of implicit scheme usually provides an overall computational advantage. Hence, for implicit scheme and Crank Nicolson scheme the problem about the computational time can be solved by choosing larger values of h and k. But there is one important aspect that can affect the computational time which is the way the implementation of the computer coding, which is different type of computer coding gives different computational time needed to solve the system equation. Here the explanation on computational time is being considered for each scheme separately. Hence it is a good idea to find and identify the fastest computational time needed by FDM's scheme to perform the solution according to the Theta formulation with same style of computer coding. The results of computational time needed by Wolfram Mathematica 8 to perform the result of concentration profile are shown in table 5.5.

Table 5.5 shows the computational time needed by Wolfram Mathematica 8 to perform the result from the three schemes of Theta formulation. These evaluations of concentration profile was done during 5 minutes of discharge with 0.5, 1.0 and 1.39 mA/cm^2 discharge current at certain number of time level calculation. Besides that this evaluation was also done by using fixed value of $h = 0.1$ and certain value of $k = 0.1$, 0.05, 0.01, 0.005, 0.001 and 0.0005. In order to get the concentration profile during 5 minutes of discharge, it needs to perform 90 time level evaluation for $k = 0.1$ and 18000 time level evaluation for $k = 0.0005$. This means that when the smaller value of k is chosen, higher time level evaluation is to be performed. The evaluation for higher time level needed more computational time to perform the concentration profile result. This can be proven by using table 5.5, which for all three schemes were shown when using the smaller value of k ($k = 0.0005$), the computational time needed are higher. For example, average computational time needed to perform the concentration profile result at $k = 0.0005$ (18000 time level evaluation) by using explicit scheme is 53.87 seconds, implicit scheme is 44.89 seconds and Crank Nicolson scheme is 54.65 seconds. It is different when we used the $k = 0.005$ (1800 time level evaluation), which show less computational time needed compared to when we used $k = 0.0005$ (18000 time level evaluation). For example, average computational time needed to perform the concentration profile result at $k = 0.005$ (1800 time level evaluation) by using explicit scheme is 5.31 seconds, implicit scheme is 4.45 seconds and Crank Nicolson scheme is 5.44 seconds.

However, when we compared the computational time needed among these three schemes for each discharge current I = 0.5, 1.0 and 1.39 mA/cm^2, we can see that the implicit scheme gives the lowest computational time needed to perform the

concentration profile result at all value of k. This implicit scheme gives the average time needed to perform the concentration profile result at k = 0.0005 (18000 time level evaluation) equal to 44.89 seconds, k = 0.005 (1800 time level evaluation) equal to 4.45 seconds and k = 0.05 (180 time level evaluation) equal to 0.42 seconds. Hence, from table 5.5, we can conclude that the smaller value of k chosen, the higher computational time needed to perform the concentration profile result. In short, the best scheme is implicit scheme because implicit scheme gives the lowest computational time needed to perform the concentration profile result compared to explicit scheme and Crank Nicolson scheme for each discharge current I = 0.5, 1.0 and 1.39 mA/cm^2.

From the comparison result of theta formulation with Doyle and Newman (1997), we find that implicit scheme from Theta formulation is the most suitable and better compared to explicit scheme and Crank Nicolson scheme. This is because implicit scheme gives the lowest computational time needed to perform concentration profile result, RMSE and MAE compared to explicit scheme and Crank Nicolson scheme. This means the implicit scheme is the fastest scheme to simulate concentration profile and the most effective and accurate scheme compared to explicit scheme and Crank Nicolson scheme.

5.3 SIMULATION OF LITHIUM-ION CELL

Having confirmed that the implicit scheme is the most suitable scheme for this study, the simulations of the concentration profiles across a lithium-ion battery system is performed. This time the plots for the concentration profile will use the parameter values that are tabulated in table 5.6.

Table 5.6: Parameters and values for Li//$LiMn_2O_4$ as reported by various worker.

Parameter (Unit)	Value	Reference
Porosity of electrode, ε	0.3	(Fuller, Doyle et al. 1994), (Garcı´a, Chiang et al. 2005), (Ali and Arof 2008)
Diffusion of coefficient, D (cm^2/s)	7.5×10^{-7}	(Doyle and Newman 1996), (Gu and Wang 1999), (Srinivasan and Wang 2003), (Ali and Arof 2008)
Faraday's constant, F (C/mol)	96487	Standard
Initial concentration, c_o (mol/cm^3)	2×10^{-3}	(Doyle and Newman 1996), (Doyle and Newman 1997), (Gu and Wang 1999)
Transference number, t_+^0	0.2	(Fuller, Doyle et al. 1994), (Doyle and Newman 1997), (Wanga and Sastry 2007), (Ali and Arof 2008)
Thickness of separator, δ_s (cm)	50×10^{-4}	(Fuller, Doyle et al. 1994), (Doyle and Newman 1997), (Ali and Arof 2008)
Thickness of cathode, δ_c (cm)	200×10^{-4}	(Fuller, Doyle et al. 1994), (Doyle and Newman 1997), (Ali and Arof 2008)

The lithium-ion concentration profiles calculated using implicit scheme from Theta Formulation using parameter values from table 5.6 are plotted in figure 5.3, figure 5.4 and figure 5.5. Figure 5.3 shows the profile for lithium-ion concentration in the solution phase during 1.75 mA/cm^2 discharge current at various values of dimensionless time, τ. Figure 5.4 shows the profile for lithium-ion concentration in the solution phase during 1.75 mA/cm^2 discharge current at various values of dimensionless distance, y. Figure 5.5 shows the profile for lithium-ion concentration in the solution phase during

1.75 mA/cm2 discharge current in 3D Simulation (across dimensionless distance, y and dimensionless time, τ together).

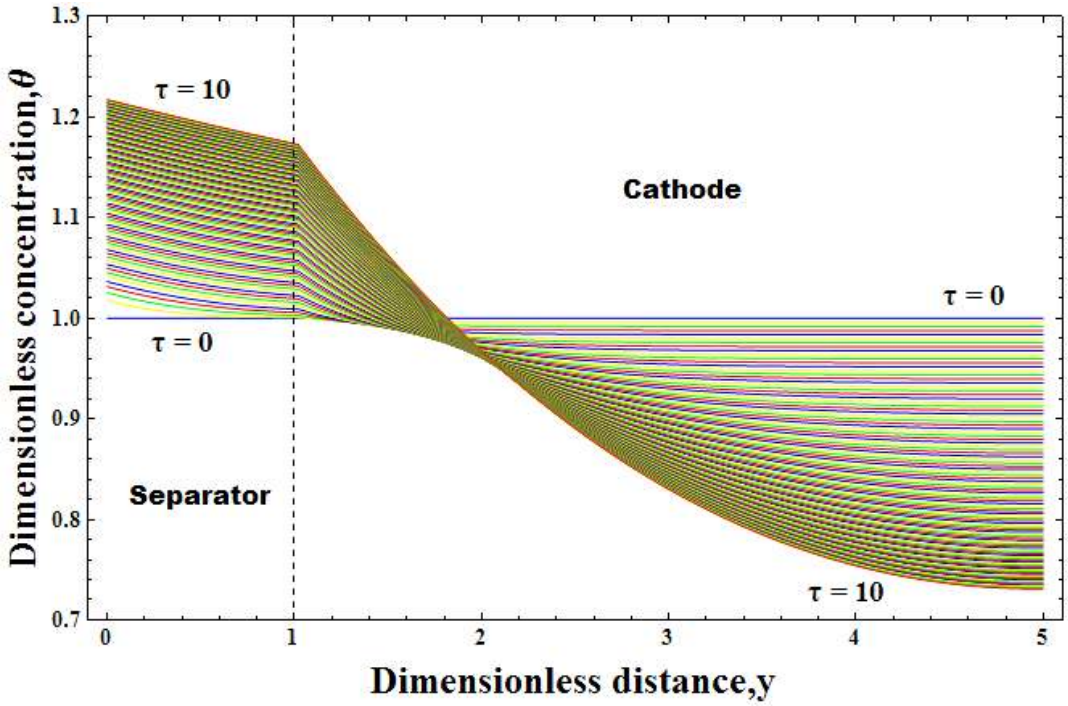

Figure 5.3: Profile for lithium-ion concentration in the solution phase during 1.75 mA/cm^2 discharge current at various values of dimensionless time, τ.

In figure 5.3, the concentration profile decreases across the dimensionless distance (separator and cathode). These concentration profiles are plotted for various values of dimensionless discharge time from τ = 0 to τ = 10 (100 concentration profiles). From figure 5.3, it can be seen that at τ = 0 there is straight line along dimensionless concentration, θ = 1.0. This is initial concentration for lithium-ion at τ = 0 because in chapter 3 it is assumed that the initial condition $\vartheta_1 = \vartheta_2 = 1$. Then at τ = 10, it can be seen that the concentration profile shows linear decreasing slope in separator region and quadratic decreasing slope in cathode region. Besides that it also can be seen the concentration profiles for discharge time, τ = 0.1 to τ = 9.9 during 1.75 mA/cm^2 discharge current from figure 5.3. The effect of discharge time towards concentration profile will be discussed later.

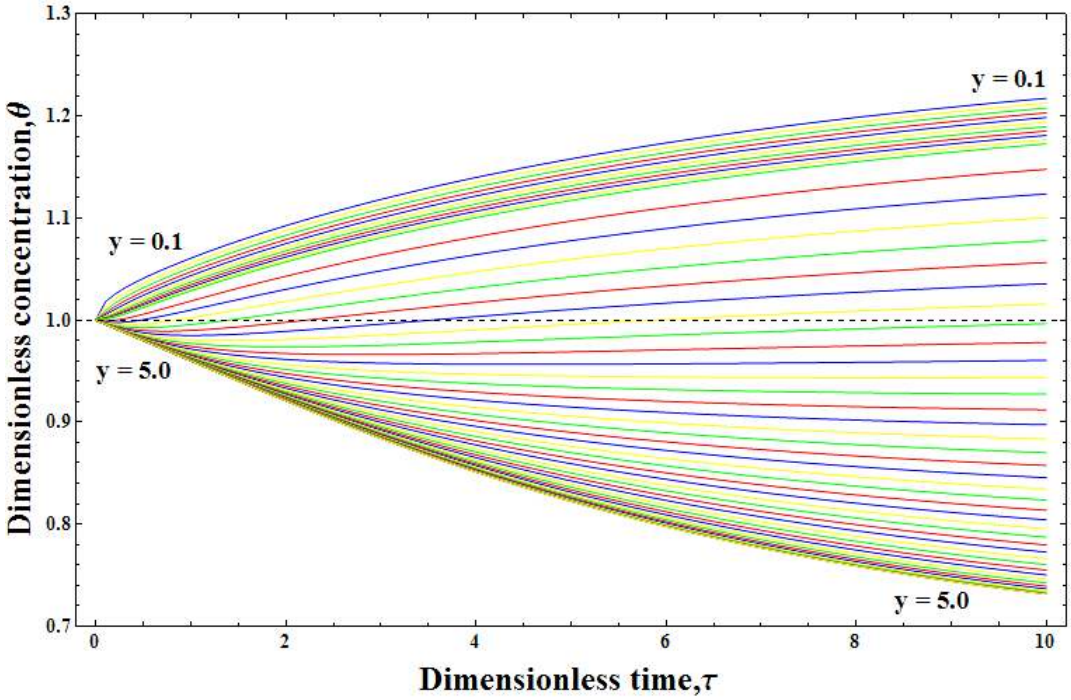

Figure 5.4: Profile for lithium-ion concentration in the solution phase during 1.75 mA/cm^2 discharge current at various values of dimensionless distance, y.

In figure 5.4, the concentration profiles are plotted for various values of dimensionless distance from y = 0.1 to y = 5.0 (50 concentration profiles). From figure 5.4, it is seen that at y = 0.1 there is quadratic increasing slope and at y = 5.0 there is quadratic decreasing slope. Besides that it can be seen that the concentration profiles shape for dimensionless distance, y = 0.2 to y = 4.9 during 1.75 mA/cm^2 discharge current from figure 5.4. The explanation about the shape of quadratic increasing and decreasing slope will be discussed later.

One of the advantages by using FDM is its ability to illustrate this model in 3-dimensional forms. Hence figure 5.5 shows the 3-dimensional plot profile for lithium-ion concentration in the solution phase during 1.75 mA/cm^2 discharge current. The

shape in simulation of profile for lithium-ion concentration in figure 5.3 and figure 5.4 can be explained well from 3-dimensional form from figure 5.5.

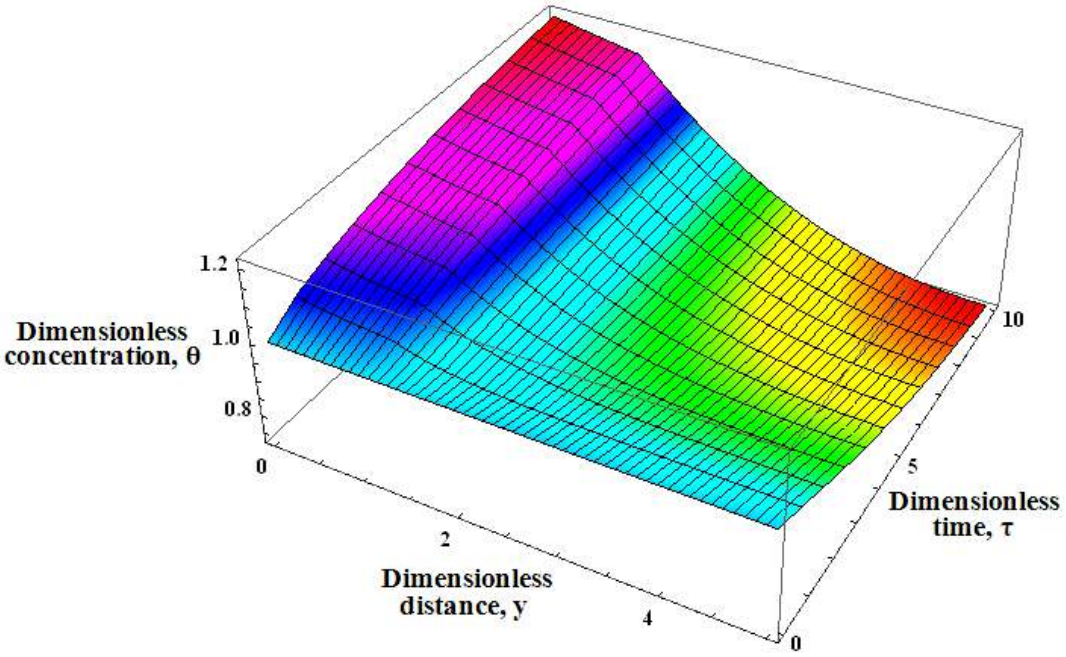

Figure 5.5: Profile for lithium-ion concentration in the solution phase during 1.75 mA/cm^2 discharge current in 3D Simulation.

From figure 5.5 the full shape of lithium-ion concentration profiles is seen because this figure included both the changes of dimensionless time and dimensionless distance. All 100 concentration profiles in figure 5.3 and 50 concentration profiles in figure 5.4 are plotted in figure 5.5 (summary for figure 5.3 and figure 5.4). In other words, all the shape are visible in figure 5.3 and figure 5.4 in figure 5.5.

Next simulation is performed in order to observe the effect of changes in other parameter values (various conditions) towards the lithium-ion concentration. The concentration profiles of lithium-ion during high and low galvanostatic discharge currents are simulated in figure 5.6.

Figure 5.6 shows the concentration profiles across cathode during galvanostatic discharge at 1.0 mA/cm^2 (figure 5.6(a)) and 1.39 mA/cm^2 (figure 5.6(b)) for various discharge times.

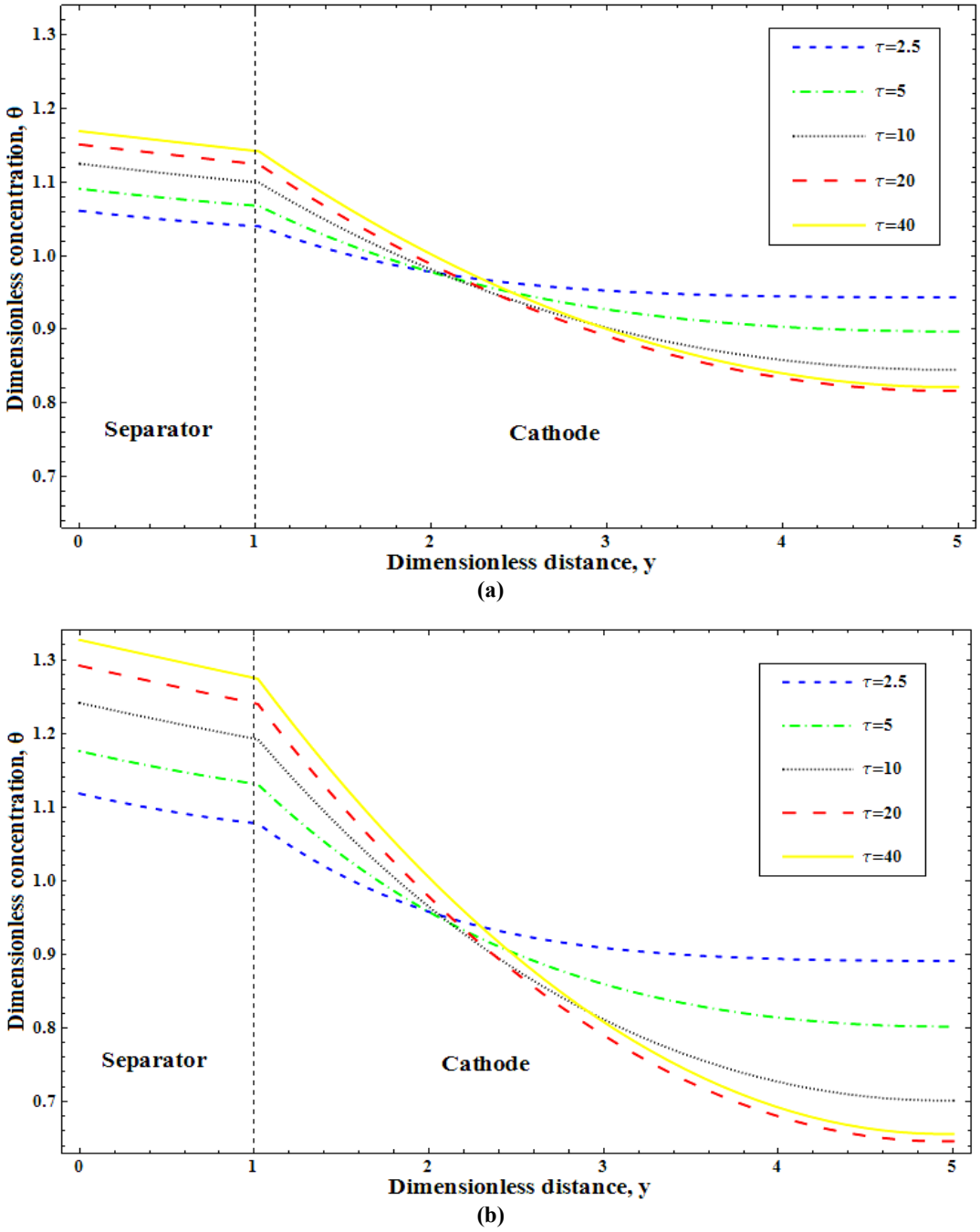

Figure 5.6: Profile for lithium-ion concentration across the cathode for different discharge times at (a) 1.0 mA/cm^2 and (b) 1.39 mA/cm^2 discharge current.

Generally, from figure 5.6(a) and figure 5.6(b), as lithium-ions diffuse across the cathode, initially, there is a decreasing profile in concentration with linear decreasing slope at separator and quadratic decreasing slope at cathode. Then the concentrations gradually become constant near the end of the cathode.

In figure 5.6(a), we can see that the initial concentration at $\tau = 2.5$ is 1.06117, $\tau = 5$ is 1.09108, $\tau = 10$ is 1.12501, $\tau = 20$ is 1.15121 and $\tau = 40$ is 1.16931. However, figure 5.6(b) shows that the initial concentration at these five time level ($\tau = 2.5$, 5, 10, 20 and 40) are higher compared to initial concentration in figure 5.6(a). These initial concentration from figure 5.6(b) are 1.11806 at $\tau = 2.5$, 1.17579 at $\tau = 5$, 1.24127 at $\tau = 10$, 1.29184 at $\tau = 20$ and 1.32676 at $\tau = 40$. In figure 5.6(a), the final concentration at $\tau = 2.5$ is 0.943473, $\tau = 5$ is 0.897287, $\tau = 10$ is 0.845268, $\tau = 20$ is 0.816504 and $\tau = 40$ is 0.821736. While, the final concentration in figure 5.6(b) are 0.890902 at $\tau = 2.5$, 0.801764 at $\tau = 5$, 0.701368 at $\tau = 10$, 0.645853 at $\tau = 20$ and 0.655951 at $\tau = 40$.

The difference between initial and final concentration define the depletion rate. Hence, from the figure 5.6(a) and 5.6(b), it is seen that at certain discharge current, the longer period of discharge time gives the higher depletion rate. For example, at discharge rate 1.0 mA/cm^2 in figure 5.6(a), it is seen that the depletion rate for shorter discharge time, $\tau = 2.5$ is lower compared to depletion rate for longer discharge time, $\tau = 20$. This phenomenon is similar for higher discharge rate 1.39 mA/cm^2 in figure 5.6(b). In addition, the difference between figure 5.6(a) and figure 5.6(b) is that the depletion rate is higher when the discharge current is higher. This means that as the discharge time increases, the concentration deplete becomes faster at the higher discharge current.

Another interesting pattern noticed in figure 5.6 is the difference in the decreasing of graph at $\tau = 40$ where the graph for $\tau = 40$ curve shifted above the graph for $\tau = 20$. This behavior was also observed by Doyle and Newman (1996), where according to them, this behavior occurred because of the graph at $\tau = 40$ have exceeded the pseudo-steady-state form. The behavior for the graph at $\tau = 40$ in (Doyle and Newman 1996) work are illustrated in figure 2.5(a) in chapter 2.

Figure 5.7(a) and figure 5.7(b) give the concentration profile for short time ($\tau = 5$) and long time ($\tau = 30$) of battery under various discharge currents. The shape of the graph is similar to that of the graphs in figure 5.6 where the concentration decreases with linear decreasing slope at separator, quadratic decreasing slope at cathode and become constant at the back of the cathode ($y = 5$).

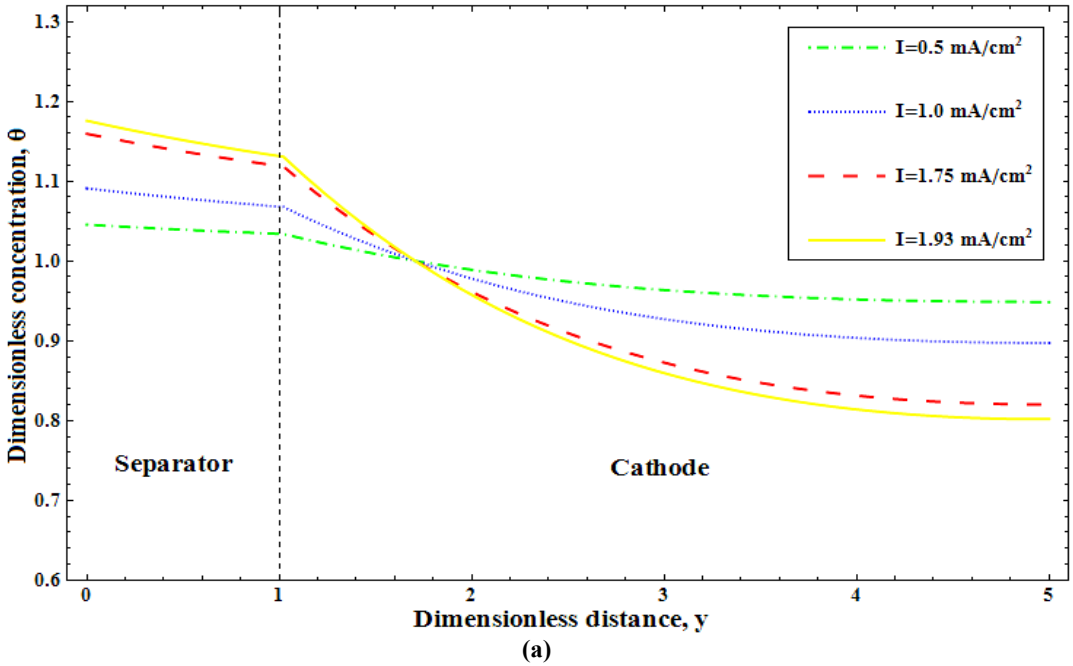

(a)

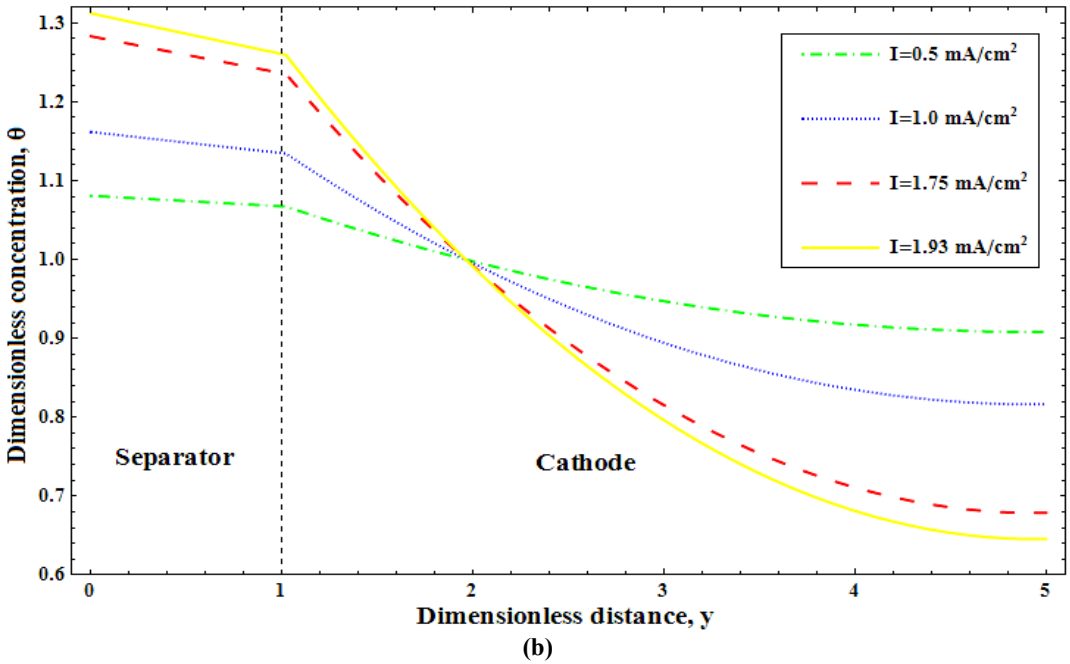

(b)

Figure 5.7: Profile for lithium-ion concentration across the cathode during (a) $\tau = 5$ and (b) $\tau = 30$ for different discharge current.

In figure 5.7(a), we can see that the initial concentration at $\tau = 5$ during discharge current I = 0.5 mA/cm^2 is 1.04554, I = 1.0 mA/cm^2 is 1.09108, I = 1.75 mA/cm^2 is 1.1594 and I = 1.93 mA/cm^2 is 1.17579. However, figure 5.7(b) shows that the initial concentration at $\tau = 30$ for these four discharge currents (I = 0.5, 1.0, 1.75 and 1.93) are higher compared to initial concentration in figure 5.7(a). The initial concentrations from figure 5.7(b) are 1.08089 during I = 0.5 mA/cm^2, 1.16179 during I = 1.0 mA/cm^2, 1.28313 during I = 1.75 mA/cm^2 and 1.31225 during I = 1.93 mA/cm^2. Meanwhile, in figure 5.7(a), the final concentration during discharge current I = 0.5 mA/cm^2 is 0.948643, I = 1.0 mA/cm^2 is 0.897287, I = 1.75 mA/cm^2 is 0.820252 and I = 1.93 mA/cm^2 is 0.801764. The final concentrations in figure 5.7(b) are 0.908162 during I = 0.5 mA/cm^2, 0.816323 during I = 1.0 mA/cm^2, 0.678565 during I = 1.75 mA/cm^2 and 0.645504 during I = 1.93 mA/cm^2. The intersection point at shorter discharge time $\tau = 5$ occurred at y = 1.7 and at longer discharge time $\tau = 30$ occurred at y = 1.9.

Hence, from figure 5.7(a) and 5.7(b), it can be observed that at certain discharge time, higher discharge current gives higher depletion rate. For example, at shorter discharge time $\tau = 5$ in figure 5.7(a), it can be seen that the depletion rate for lower discharge current, I = 0.5 mA/cm^2 is lower compared to the depletion rate for higher discharge current, I = 1.93 mA/cm^2. This phenomenon is similar for longer discharge time $\tau = 30$ in figure 5.7(b). In addition, the difference between figure 5.7(a) and figure 5.7(b) is the depletion rate is higher when the discharge time is longer. This means that as the discharge current increases, the concentration depletes faster for longer discharge time.

In figure 5.8, the concentration profiles for 5 different distances, ***r*** in cathode are plotted. These plots allow us to observe the amount of lithium-ions at certain distance of cathode. Figure 5.8(a) shows that the concentration profile for 1.0 mA/cm^2 and figure 5.8(b) for 1.93 mA/cm^2 discharge current.

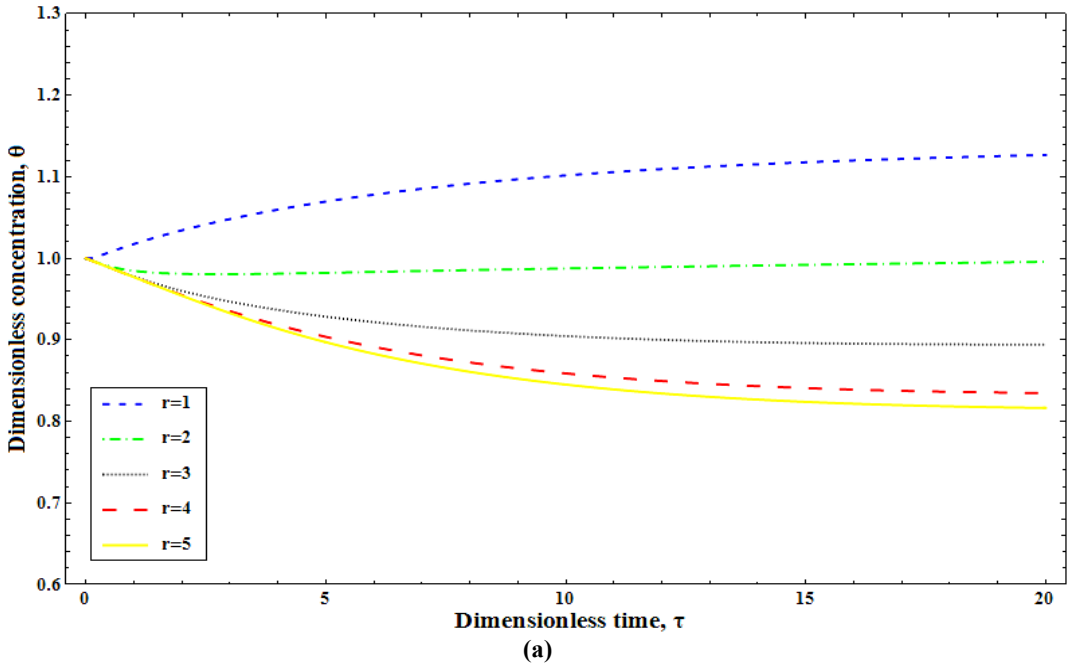

(a)

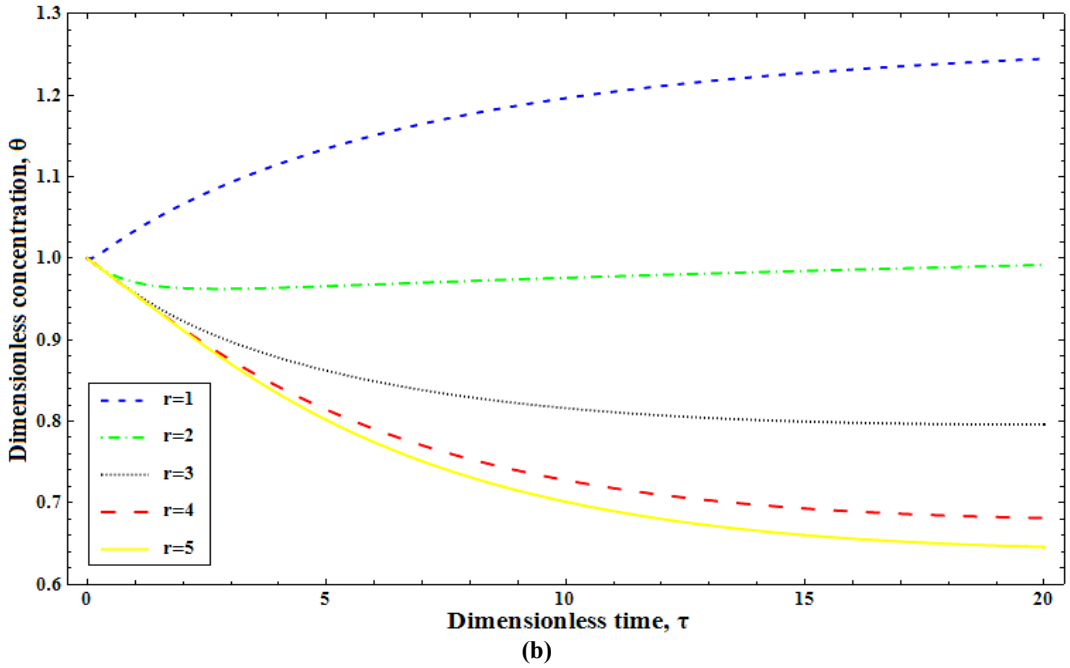

(b)

Figure 5.8: Profile for lithium-ion concentration across the cathode at different distance, *r* using (a) 1.0 mA/cm^2 and (b) 1.93 mA/cm^2 discharge current.

From figure 5.8(a) and figure 5.8(b), the initial concentration for all distances (***r*** = 1, 2, 3, 4 and 5) are 1 because from chapter 3, we have assumed the initial condition $\vartheta_1 = \vartheta_2 = 1$. The final concentration in figure 5.8(a) at ***r*** = 1 is 1.12686, ***r*** = 2 is 0.995805, ***r*** = 3 is 0.894293, ***r*** = 4 is 0.834848 and ***r*** = 5 is 0.816504. Meanwhile, the final concentration in figure 5.8(b) at ***r*** = 1 is 1.24484, ***r*** = 2 is 0.991904, ***r*** = 3 is 0.795986, ***r*** = 4 is 0.681257 and ***r*** = 5 is 0.645853.

From these two figures, it can be deduced that, at the front of the cathode (***r*** = 1), the shape of concentration profile is quadratic increasing slope. This means the concentration increases with time. This is because more lithium-ions have dissolved from the separator into the front of the cathode. However, at ***r*** = 2, the concentration still increases with quadratic increasing slope but at a lower rate than the increment at ***r*** = 1. This means that the amount of lithium-ion dissolved from the separator (***r*** = 1) is

still higher then amount of lithium-ion in the cathode. If it is observed carefully, there is a slight decay behavior at $\boldsymbol{r} = 2$ during discharge process ($\tau = 0$) to ($\tau = 2$). Before the discharge process there are also some leftover lithium-ion in the system causing us to assume the initial condition to be equal to $\vartheta_1 = \vartheta_2 = 1$ (uniform initial condition). At the beginning of the discharge process, the leftover lithium-ion at $\boldsymbol{r} = 2$ will be used first before more lithium-ions starts to flow in from the anode-separator. Thus, this cause the slight decay in lithium-ion concentration at time interval $\tau = 0$ to $\tau = 2$. Then, for $\boldsymbol{r} = 3$, $\boldsymbol{r} = 4$ and $\boldsymbol{r} = 5$ the concentrations start to decrease (quadratic decreasing slope) because the lithium-ions have already combined with active material of the electrode through chemical reaction (reduction process). The decreases at $\boldsymbol{r} = 5$ is greater than $\boldsymbol{r} = 4$ and $\boldsymbol{r} = 3$ because the position of $\boldsymbol{r} = 5$ are at the back of the cathode. Hence, we know that the reduction process are more active at $\boldsymbol{r} = 5$ then at $\boldsymbol{r} = 4$ and $\boldsymbol{r} = 3$.

From figure 5.6 to figure 5.8, we have discussed the connection and behavior of the lithium-ion concentration profiles involved the discharge time (τ), discharge current (I) and position in battery ($\boldsymbol{r}$). Now, we want to simulate the concentration profiles of lithium-ion for high and low electrode porosity, ε. Figure 5.9(a) and figure 5.9(b) give the concentration profiles during specific discharge current at high ($\varepsilon = 0.8$) and low ($\varepsilon = 0.2$) electrode porosity for various discharge times.

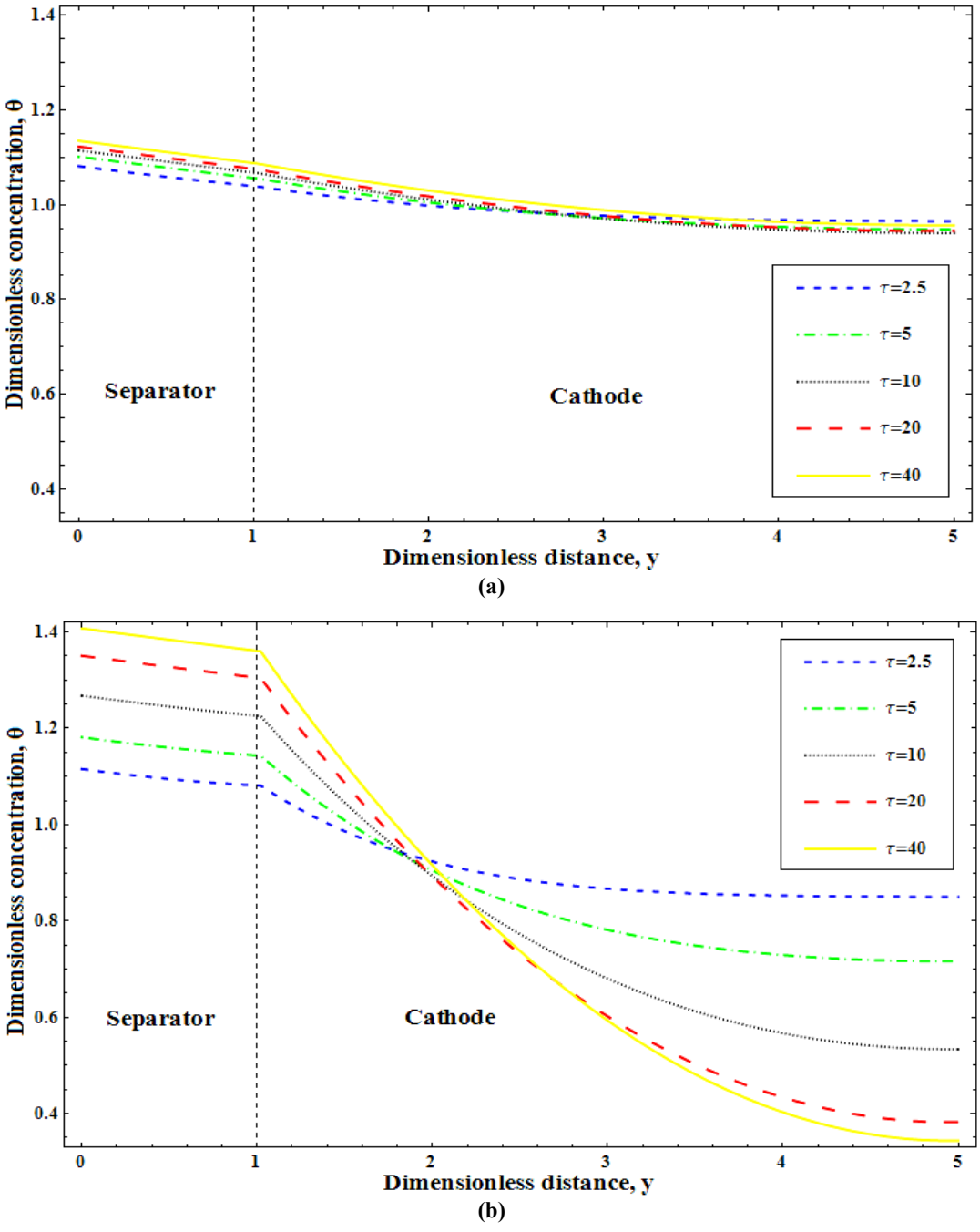

Figure 5.9: Profile for lithium-ion concentration across the cathode at certain discharge current for different discharge times with electrode porosity (a) ε = 0.8 and (b) ε = 0.2.

Figure 5.9(a) shows that the concentration profiles decrease slowly and exhibit an almost linear slope. Figure 5.9(b) shows that the concentration profiles decrease with linear decreasing slope at separator, quadratic decreasing slope at cathode and become

almost constant at the back of the cathode. In figure 5.9(a), we can see that the initial concentration at $\tau = 2.5$ is 1.08155, $\tau = 5$ is 1.10156, $\tau = 10$ is 1.11475, $\tau = 20$ is 1.12274 and $\tau = 40$ is 1.13506. However, figure 5.9(b) shows that the initial concentration at these five discharge times level ($\tau = 2.5$, 5, 10, 20 and 40) are higher compared to initial concentration in figure 5.9(a). These initial concentrations from figure 5.9(b) are 1.11546 at $\tau = 2.5$, 1.18135 at $\tau = 5$, 1.2677 at $\tau = 10$, 1.35052 at $\tau = 20$ and 1.40739 at $\tau = 40$. In figure 5.9(a), the final concentration at $\tau = 2.5$ is 0.965455, $\tau = 5$ is 0.947993, $\tau = 10$ is 0.940287, $\tau = 20$ is 0.944446 and $\tau = 40$ is 0.956671. The final concentrations in figure 5.9(b) are 0.850321 at $\tau = 2.5$, 0.716274 at $\tau = 5$, 0.533862 at $\tau = 10$, 0.382341 at $\tau = 20$ and 0.343953 at $\tau = 40$.

Recall that, the difference between initial and final concentration define as the deplete rate. Hence, from the figure 5.9(a) and 5.9(b), it is seen that at certain electrode porosity, longer discharge time gives higher depletion rate. For example, for high electrode porosity, $\varepsilon = 0.8$, in figure 5.9(a), it is seen that the depletion rate for shorter discharge time ($\tau = 2.5$) is lower compared to depletion rate for longer discharge time ($\tau = 10$). In low electrode porosity, $\varepsilon = 0.2$, in figure 5.9(b), it is seen that the depletion rate for shorter discharge time ($\tau = 2.5$) is lower compared to depletion rate for higher discharge time ($\tau = 40$). It is also observed that the depletion rate is higher when porosity of electrode is lower ($\varepsilon = 0.2$). This means that as the discharge time increases, concentration deplete faster in lower electrode porosity compared to in higher electrode porosity.

In figure 5.9(a), there is a different pattern in the decreasing trend of graph at $\tau = 20$ and $\tau = 40$ where the curves for these two graphs shifted above than other three graphs ($\tau = 2.5$, $\tau = 5$ and $\tau = 10$). This behavior was also observed by Doyle and

Newman (1996), where according to them, this behavior occurred because of the graph at $\tau = 20$ and $\tau = 40$ has exceed the pseudo-steady-state form. The behavior for the graph at $\tau = 40$ in Doyle and Newman (1996) work are illustrated in figure 2.5(a) at chapter 2. However, in figure 5.9(b), there is no pseudo-steady-state form behavior occurs at $\tau = 20$ and $\tau = 40$. Hence, this means the higher electrode porosity make the pseudo-steady-state form behavior to occur faster than lower electrode porosity.

Now, we want to see the relation between electrode porosity with discharge current. Hence, Figure 5.10(a) and figure 5.10(b) give the concentration profiles during specific discharge time at high ($\varepsilon = 0.8$) and low ($\varepsilon = 0.2$) electrode porosity for various discharge currents.

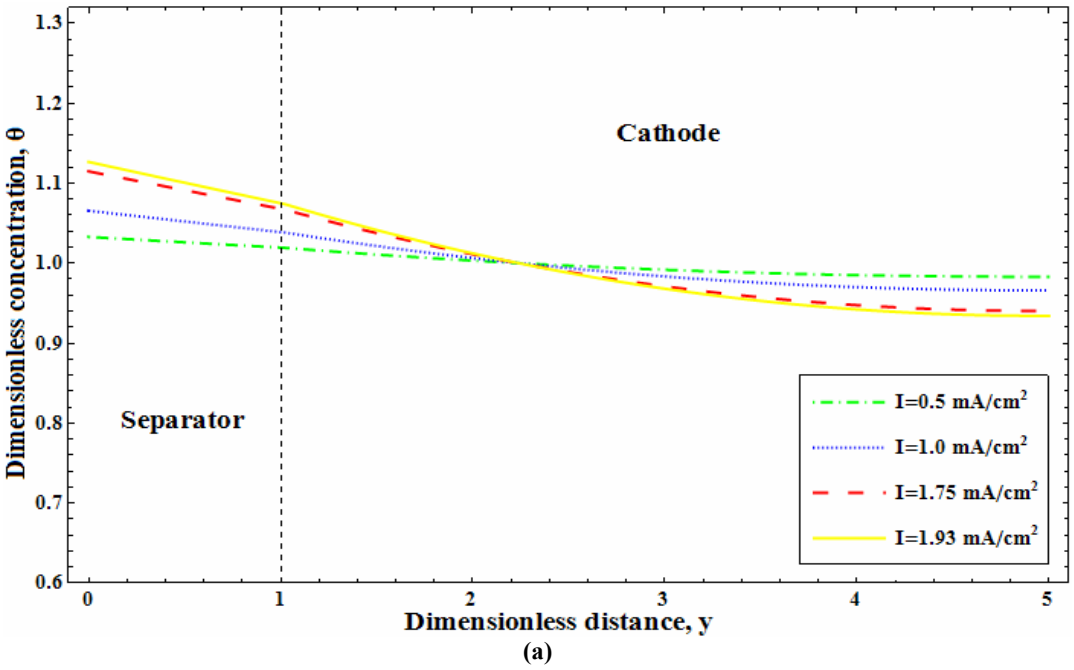

(a)

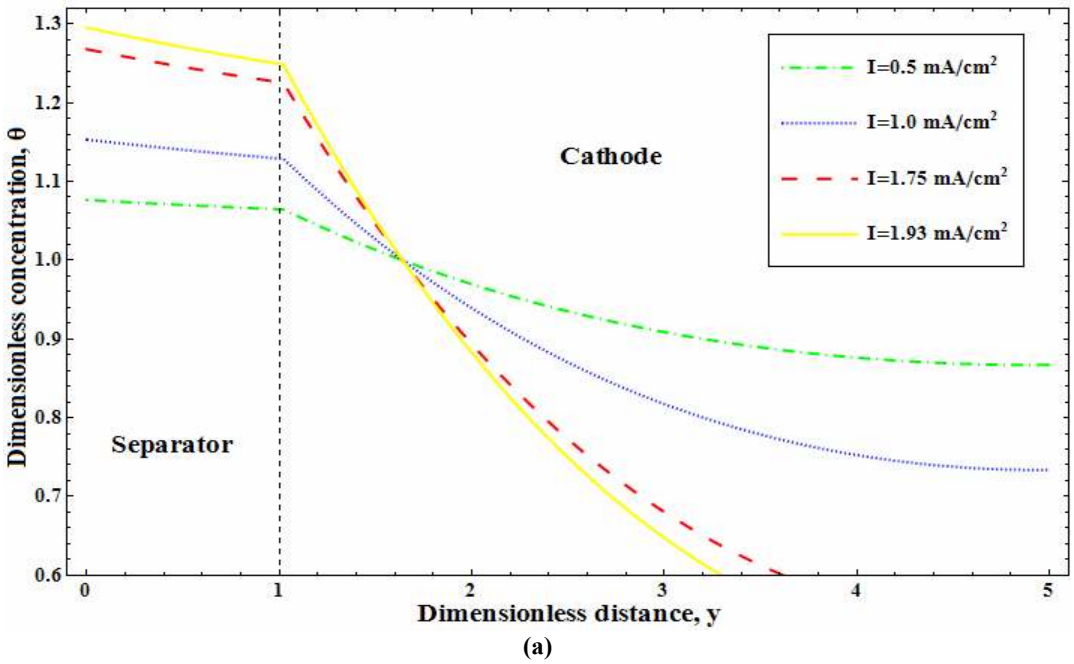

(a)

Figure 5.10: Profile for lithium-ion concentration across the cathode during certain discharge time for different discharge current with electrode porosity (a) ε = 0.8 and (b) ε = 0.2.

Figure 5.10(a) shows that the concentration profiles decrease slowly and exhibit an almost linear slope. However, figure 5.10(b) shows that the concentration profiles decrease with linear decreasing slope at separator, quadratic decreasing slope at cathode and become constant at the back of the cathode. In figure 5.10(a), we can see that the initial concentration at I = 0.5 mA/cm^2 is 1.03278, I = 1.0 mA/cm^2 is 1.06557, I = 1.75 mA/cm^2 is 1.11475 and I = 1.93 mA/cm^2 is 1.12655. In figure 5.10(b), the initial concentration at these four discharge currents (I = 0.5, 1.0, 1.75 and 1.93 mA/cm^2) are higher compared to initial concentration in figure 5.10(a). These initial concentration from figure 5.10(b) are 1.07649 at I = 0.5 mA/cm^2, 1.15297 at I = 1.0 mA/cm^2, 1.2677 at I = 1.75 mA/cm^2 and 1.29524 at I = 1.93 mA/cm^2. In figure 5.10(a), the final concentration at I = 0.5 mA/cm^2 is 0.982939, I = 1.0 mA/cm^2 is 0.965879, I = 1.75 mA/cm^2 is 0.940287 and I = 1.93 mA/cm^2 is 0.934146. Beside that, the final

concentration in figure 5.10(b) are 0.866818 at I = 0.5 mA/cm^2, 0.733635 at I = 1.0 mA/cm^2, 0.533862 at I = 1.75 mA/cm^2 and 0.485916 at I = 1.93 mA/cm^2.

From figure 5.10(a) and 5.10(b), it can be seen that at certain electrode porosity, higher discharge current gives higher depletion rate. For example, for high electrode porosity, ε = 0.8, in figure 5.10(a), that the depletion rate for lower discharge current, I = 0.5 mA/cm^2 is lower compared to depletion rate for higher discharge current, I = 1.93 mA/cm^2. In low electrode porosity, ε = 0.2, in figure 5.10(b), that the depletion rate for lower discharge current, I = 0.5 mA/cm^2 is lower compared to depletion rate for higher discharge current, I = 1.93 mA/cm^2. Besides that, from these two figures (figure 5.10(a) and figure 5.10(b)), the depletion rate is higher when electrode porosity is lower (ε = 0.2). This means that as the discharge current increases, concentration deplete faster in lower electrode porosity compared to in higher electrode porosity.

In figure 5.11, the concentration profiles for different distances, ***r*** in cathode are plotted to observe the amount of lithium-ions at certain distance of cathode. Figure 5.11(a) shows the concentration profiles for electrode porosity, ε = 0.8 and figure 5.11(b) for porosity, ε = 0.2.

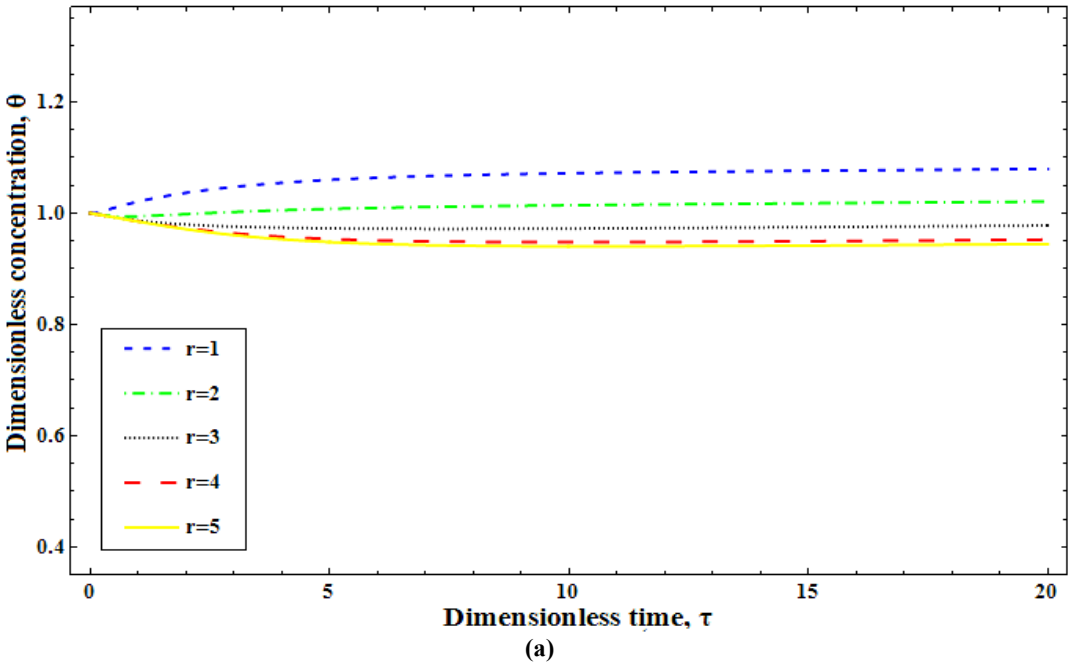

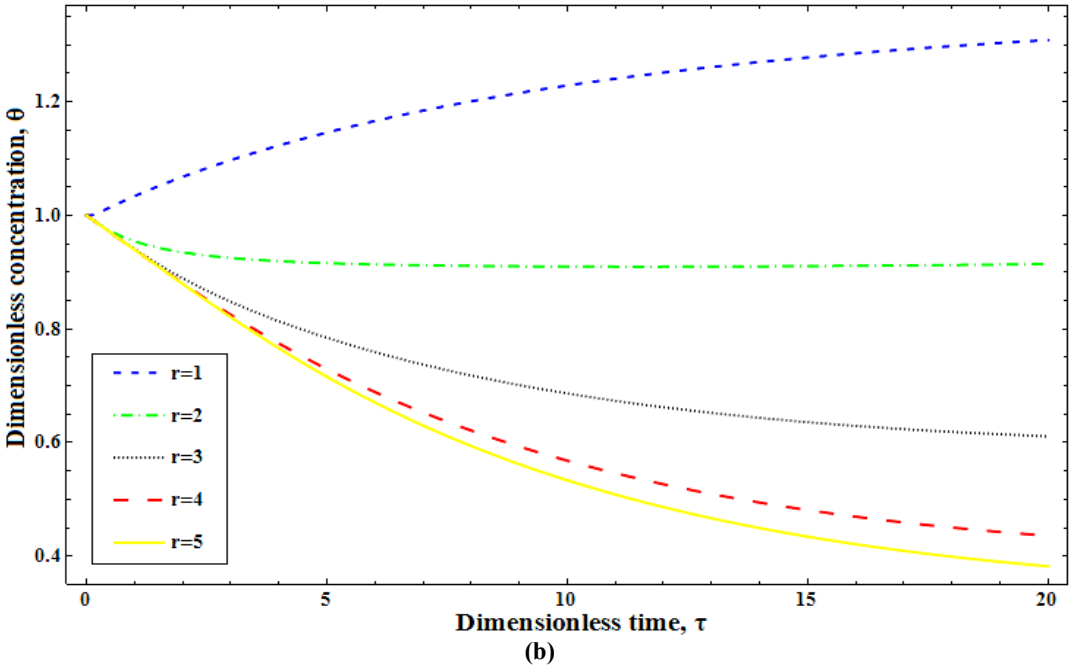

Figure 5.11: Profile for lithium-ion concentration across the cathode for different distance, *r* using electrode porosity (a) ε = 0.8 and (b) ε = 0.2 at certain discharge current.

From these two figure (figure 5.11(a) and figure 5.11(b)), the initial concentration for all distances (***r*** = 1, 2, 3, 4 and 5) is 1 because from chapter 3, it is assumed the initial condition $\vartheta_1 = \vartheta_2 = 1$. The final concentration in figure 5.11(a) at ***r***

= 1 is 1.07944, ***r*** = 2 is 1.02087, ***r*** = 3 is 0.977822, ***r*** = 4 is 0.95235 and ***r*** = 5 is 0.944446. Meanwhile, the final concentration in figure 5.11(b) at ***r*** = 1 is 1.3088, ***r*** = 2 is 0.914411, ***r*** = 3 is 0.611176, ***r*** = 4 is 0.436004 and ***r*** = 5 is 0.382341.

These two figures show that when electrode porosity decreases the concentration at ***r*** = 1 increases, concentration at ***r*** = 2 increases slightly. A part of that the concentration at ***r*** = 1 and ***r*** = 2 increase with increasing dimensionless time. However concentration at ***r*** = 3, ***r*** = 4 and ***r*** = 5 decreases. For concentration at ***r*** = 3, ***r*** = 4 and ***r*** = 5, as the dimensionless time increases the concentration decreases. All the increasing concentration profiles (***r*** = 1 and ***r*** = 2), decreasing concentration profiles (***r*** = 3, ***r*** = 4 and ***r*** = 5) and decay behavior (at ***r*** = 2 during $\tau = 0$ to $\tau = 2$) occurs in figure 5.11 have been explained in explanation for figure 5.8.

In addition, from these two figures, low porosity of electrode gives higher increasing rate of concentration profile at ***r*** = 1 and ***r*** = 2 compare to high porosity of electrode. However, low porosity of electrode gives higher decreasing rate of concentration profile at ***r*** = 3, ***r*** = 4 and ***r*** = 5 compare to high porosity of electrode.

Thickness of separator and cathode also play a major effect towards the concentration of lithium-ion in lithium-ion battery during discharge. Thus figure 5.12 shows the combinations of five different thicknesses of cathode and separator.

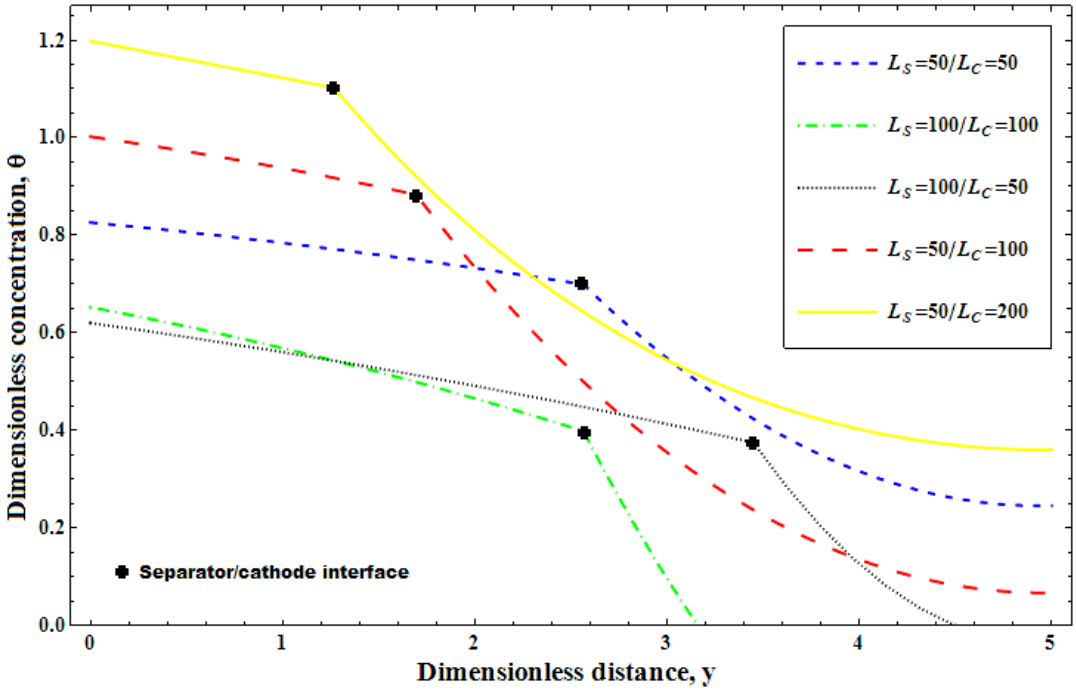

Figure 5.12: Profile for lithium-ion concentration for 5 different thicknesses combination of separator and cathode. The thicknesses of separator and cathode are measured in μm during certain discharge current and time.

From figure 5.12, as lithium-ions diffuse across the cathode, initially, there is a decrease in concentration with linear decreasing slope at separator and quadratic decreasing slope at cathode. So all the five concentration profiles for different thicknesses of separator and cathode combination in figure 5.12 shows a normal decreasing slope shape, which is linear decreasing slope at separator and quadratic decreasing slope at cathode.

In figure 5.12, we can see that the initial concentration for separator and cathode thickness combination, $\frac{\delta_C}{\delta_S}=\frac{50}{50}$ is 0.82637, $\frac{\delta_C}{\delta_S}=\frac{100}{100}$ is 0.65274, $\frac{\delta_C}{\delta_S}=\frac{100}{50}$ is 0.62035, $\frac{\delta_C}{\delta_S}=\frac{50}{100}$ is 1.00220 and $\frac{\delta_C}{\delta_S}=\frac{50}{200}$ is 1.19848. Then, the final concentration

for separator and cathode thickness combination, $\frac{\delta_C}{\delta_S} = \frac{50}{50}$ is 0.24582, $\frac{\delta_C}{\delta_S} = \frac{100}{100}$ is -0.50836, $\frac{\delta_C}{\delta_S} = \frac{100}{50}$ is -0.03067, $\frac{\delta_C}{\delta_S} = \frac{50}{100}$ is 0.06739 and $\frac{\delta_C}{\delta_S} = \frac{50}{200}$ is 0.36028.

The best amongst these five different combinations for cathode and separator thicknesses is the thickness for cathode must be larger than separator in order to get slower depletion time. In addition, the larger ratio of $\frac{\delta_C}{\delta_S}$, the time depletion of lithium-ion is much slower. These are agreeable with several batteries in the industry (Johnson and White 1998), where the cathode thickness must be larger than the separator thickness to get slower depletion rate.

Table 5.2: *p* value from t-test (significant test) compared to Doyle & Newman (1997) for 5 minutes of discharge with 0.5, 1.0 and 1.39 mA/cm^2 discharge current for three schemes in Theta formulation.

***t*-test p-value (significance test) compared to Doyle & Newman (1997) for 5 minutes of discharge**							
Current (mA/cm^2)	**FDM Scheme**	***k***					
		0.0005	**0.001**	**0.005**	**0.01**	**0.05**	**0.1**
0.5	**Explicit**	0.482136	0.482321	0.483802	unstable	unstable	unstable
	Crank Nicolson	0.482042	0.482133	0.482860	0.483769	0.491045	0.499849
	Implicit	0.481948	0.481945	0.481918	0.481885	0.481613	0.481259
1.0	**Explicit**	0.494606	0.494790	0.496255	unstable	unstable	unstable
	Crank Nicolson	0.494513	0.494603	0.495324	0.496225	0.496565	0.487549
	Implicit	0.494420	0.494417	0.494392	0.494361	0.494109	0.493779
1.39	**Explicit**	0.495822	0.496005	0.497469	unstable	unstable	unstable
	Crank Nicolson	0.495729	0.495819	0.496539	0.497438	0.495360	0.486354
	Implicit	0.495636	0.495633	0.495608	0.495577	0.495327	0.494999

Table 5.3: RMSE compared to Doyle & Newman (1997) for 5 minutes of discharge with 0.5, 1.0 and 1.39 mA/cm^2 discharge current for three techniques in Theta formulation.

RMSE compared to Doyle & Newman (1997) for 5 minutes of discharge							
Current (mA/cm^2)	**FDM Scheme**	***k***					
		0.0005	**0.001**	**0.005**	**0.01**	**0.05**	**0.1**
0.5	**Explicit**	0.0153180	0.0153122	0.0152676	unstable	unstable	unstable
	Crank Nicolson	0.0153177	0.0153117	0.0152636	0.0152044	0.0147656	0.0143112
	Implicit	0.0153175	0.0153112	0.0152609	0.0151981	0.0147027	0.0141028
1.0	**Explicit**	0.0189773	0.0189707	0.0189227	unstable	unstable	unstable
	Crank Nicolson	0.0189757	0.0189674	0.0189025	0.0188245	0.0183336	0.0180712
	Implicit	0.0189742	0.0189643	0.0188860	0.0187891	0.0180526	0.0172434
1.39	**Explicit**	0.0227376	0.0227287	0.0226649	unstable	unstable	unstable
	Crank Nicolson	0.0227347	0.0227226	0.0226281	0.0225151	0.0218251	0.0215345
	Implicit	0.0227318	0.0227168	0.0225973	0.0224494	0.0213238	0.0200874

Table 5.4: MAE compared to Doyle & Newman (1997) for 5 minutes of discharge with 0.5, 1.0 and 1.39 mA/cm^2 discharge current for three techniques in Theta formulation.

MAE compared to Doyle & Newman (1997) for 5 minutes of discharge							
Current (mA/cm^2)	**FDM Scheme**	***k***					
		0.0005	**0.001**	**0.005**	**0.01**	**0.05**	**0.1**
0.5	**Explicit**	0.0130609	0.0130595	0.0130483	unstable	unstable	unstable
	Crank Nicolson	0.0130590	0.0130557	0.0130292	0.0129960	0.0127290	0.0124418
	Implicit	0.0130571	0.0130518	0.0130100	0.0129578	0.0125372	0.0120150
1.0	**Explicit**	0.0176838	0.0176774	0.0176264	unstable	unstable	unstable
	Crank Nicolson	0.0176827	0.0176752	0.0176155	0.0175406	0.0169503	0.0162328
	Implicit	0.0176816	0.0176731	0.0176045	0.0175188	0.0168291	0.0160033
1.39	**Explicit**	0.0206785	0.0206721	0.0206265	unstable	unstable	unstable
	Crank Nicolson	0.0206751	0.0206653	0.0205870	0.0204890	0.0197388	0.0187978
	Implicit	0.0206717	0.0206585	0.0205529	0.0204207	0.0194254	0.0183432

Table 5.5: Computational time needed by Wolfram Mathematica 8 to perform the result of concentration profile during 5 minutes of discharge with 0.5, 1.0 and 1.39 mA/cm^2 discharge current for three techniques in Theta formulation.

Computational time in seconds to solved the system for 5 minutes of discharge							
Current (mA/cm^2)	**FDM Scheme**	**number of time level (k)**					
		18000 (0.0005)	**9000 (0.001)**	**1800 (0.005)**	**900 (0.01)**	**180 (0.05)**	**90 (0.1)**
0.5	**Explicit**	54.58	26.63	5.34	unstable	unstable	unstable
	Crank Nicolson	54.86	27.67	5.36	2.86	0.53	0.27
	Implicit	44.78	22.22	4.53	2.22	0.42	0.23
1.0	**Explicit**	53.41	27.59	5.34	unstable	unstable	unstable
	Crank Nicolson	54.52	27.41	5.41	2.73	0.53	0.27
	Implicit	44.59	22.50	4.41	2.22	0.41	0.23
1.39	**Explicit**	53.63	26.70	5.23	unstable	unstable	unstable
	Crank Nicolson	54.58	27.36	5.55	2.67	0.55	0.25
	Implicit	45.30	22.20	4.42	2.23	0.42	0.22
Average	**Explicit**	53.87	26.97	5.31	-----	-----	-----
	Crank Nicolson	54.65	27.48	5.44	2.76	0.54	0.26
	Implicit	44.89	22.31	4.45	2.22	0.42	0.23

Ali, S. A. H. and A. K. Arof (2008). "Modeling of discharge behavior of a lithium ion cell." Journal of Alloys and Compounds **449**: 292-295.

Doyle, M. and J. Newman (1996). "Comparison of Modeling Predictions with Experimental Data from Plastic Lithium Ion Cells." Journal of Electrochemical Society **143**(6): 1890-1903.

Doyle, M. and J. Newman (1997). "Analysis of capacity-rate data for lithium batteries using simplified models of the discharge process " Journal of Electrochemistry **27**: 846-856.

Fuller, T. F., M. Doyle, et al. (1994). "Simulation and Optimization of the Dual Lithium Ion Insertion Cell." Journal of Electrochemical Society **141**(1): 1-9.

Garcı´a, R. E., Y.-M. Chiang, et al. (2005). "Microstructural Modeling and Design of Rechargeable Lithium-Ion Batteries." Journal of Electrochemical Society **152**(1): 255-263.

Gu, W. B. and C. Y. Wang (1999). "Thermal-electrochemical Coupled Modeling Of a Lithium-ion Cell."

Srinivasan, V. and C. Y. Wang (2003). "Analysis of Electrochemical and Thermal Behavior of Li-Ion Cells." Journal of The Electrochemical Society **150**(1): 98-106.

Wanga, C.-W. and A. M. Sastry (2007). "Mesoscale Modeling of a Li-Ion Polymer Cell." Journal of Electrochemical Society **154**(11): 1035-1047.